ACS OMEGA

Open Access

http://pubs.acs.org/journal/acsodf

Article

Heat Transfer of Ca $(NO_3)_2$-KNO_3 Molten Salt Mixtures for Austempering and Martempering Processes of Steels

Jaimon D. Quadros, Sher Afghan Khan, Ma Mohin, Yakub I. Mogul, Abdul Aabid,* Muneer Baig, and Omar Shabbir Ahmed

Cite This: *ACS Omega* 2024, 9, 17266−17275

Read Online

ACCESS | Metrics & More | Article Recommendations

ABSTRACT: Molten salts are highly effective as a quenching medium for austempering and martempering processes, enabling precise control of cooling rates to achieve the desired microstructures and mechanical characteristics in steel components. One such promising molten salt is a multicomponent Ca $(NO_3)_2$-KNO_3 molten salt. The current work explores the cooling severity of molten Ca $(NO_3)_2$-KNO_3 mixtures, which are commonly used for such purposes. The said mixture, with varying concentrations and bath temperatures was used for quenching the Inconel probe with thermocouples. The temperature data extracted was used to determine the transient heat flux developed at the metal−quenchant interface. A set of critical points were assessed against the peak heat extraction rates. Additionally, the fluctuation of mean heat flux and surface temperature in relation to these crucial points were plotted, along with changes in composition and bath temperature of the quench media. The cooling intensity of these quench solutions, as measured by Inconel probes, correlated well with the average hardness values observed in steel probes. The level of homogeneity in heat transmission, as measured by the spatial variance of the normalized heat energy, decreased as the percentage of KNO_3 in the quench medium increased.

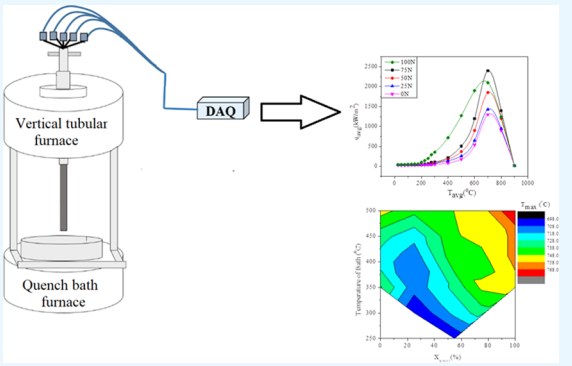

1. INTRODUCTION

For decades, quenching heat treatment was employed to enhance the hardness and resilience of steel components. Totten and Bates[1] examined the current condition of the traditional quench hardening procedure used in the heat treatment industry and found that austenitic steel parts are rapidly cooled in water, mineral and vegetable oils, and aqueous polymer mixture kept at room temperature. Narazaki et al.[2] investigated the formation of residual stress in quenched components and noticed the conversion of austenite to alternate phases during quench hardening triggers the formation of thermodynamic and transformational stresses within the component after it has been quenched. In the quenching of hardened steel components, these stresses combine to generate deformation, residual stress, fractures, and other related deficiencies. Defects reported in steel components exposed to typical quench hardening heat treatment often include distortion, residual stress, and cracking.[2]

The ASM Handbook Committee[3] defines austempering and martempering as heat treatment methods that are extensively employed for hardening steel components with little deformation, residual stress, and cracking when reviewing numerous industrial steel methods of heat treatment. The bainitic alteration temperature of the austenitized steel component is maintained for an adequate amount of time to convert all austenite to bainite. The austenitic steel component, quenched and maintained at a temperature slightly higher than the martensitic start point, is held for a brief period during martempering. When the temperature difference in the steel component becomes very low, it is withdrawn from the quenching medium and exposed to air cooling. Austenite is, therefore, allowed to transform into martensite gradually. As a result, there is a necessity to operate the quench medium temperature in the temperature range of 150−600 °C for heat treatment techniques such as austempering and martempering. Such cooling mediums are intended to provide adequate cooling rates to preclude the diffusion-based transition of austenite to pearlite, ferrite, and, in numerous instances, bainite. Quenching, on the other hand, involves key stages to impart mechanical properties to the metals. The heating of the material transforms it into an austenitic microstructure and thereafter soaks it to

Received: December 22, 2023
Revised: March 15, 2024
Accepted: March 20, 2024
Published: April 5, 2024

ensure uniformity before rapid cooling or quenching, using mediums like water, oil, polymers, etc. This quick cooling confirms the formation of martensite, contributing to increased hardness and strength.[1,3]

Molten salt quenchants have their own set of advantages when compared to the other quenchants, such as rapid cooling rate, lower distortion, less cracking, consistent and repeatable results, lower fire hazards, etc.[4] Lantelme and Groult[4] provided vital information on several technical uses of molten salts. When it comes to the utilization of molten solutions in heat treatment industries, the study indicates that, depending on the salt's structure, the bath might be used as a basic heat transmission medium or a chemically processed material at elevated temperature, in which chemical reactions between the bath and the treated component led to critical changes in structure. Dexter[5] described how molten chloride-based salt media is used for hardening high-speed steels. According to the findings, ternary combinations of sodium, potassium, and barium chlorides are often utilized as quench medium for operating bath temperatures ranging from 425−700 °C. Torkamani et al.[6] examined the hardening performance of AISI D2 steel with hot oil and NaOH-KOH combinations. The application of molten alkali chloride for quenching is limited to the heat treatment of high-speed steels, where the quenching process occurs within a controlled quenchant temperature ranging from 450−600 °C. Lisicic et al.[7] evaluated various quench media at higher temperatures used in commercial heat treatment procedures and determined that parts cooled in molten alkali hydroxides and carbonates were particularly vulnerable to oxidation and, therefore, were not preferred. Because NO_3−NO_2-based alkali combinations have an operating temperature range of 150−595 °C, they are popular industrial quench media for hardening steels. Dubal[8] conducted a thorough examination of the use of nitrite/nitrate-based molten salts for commercial purposes. He recommended maintaining the operational temperature of the quench media above the melting point of the combination, setting it at a minimum of 55 °C. The study looked at how various process factors affected the cooling effectiveness of a molten salt combination. Nonetheless, the lack of uniformity in cooling over the probe's surface was not taken into consideration in this study. The inverse heat transfer approach is a strong tool that has recently been used to investigate quenching heat transfer. Yagov et al.[9] investigated the cooling responses of various alloy steels quenched in water after being heated to 700−750 °C. They incorporated the inverse heat transfer technique to compute the heat flux and surface temperature. The investigation revealed significantly enhanced heat transfer levels in the film boiling phase, as water subcooling surpassed 20 °C in a pressurized water system operating at 100−150 °C.

Contrary to popular opinion, film boiling provides poor cooling rates throughout the quench heat transfer. Pranesh Rao and Prabhu[10] incorporated the inverse heat transfer technique to determine the transient quench heat flux that was spatially based. Their aim was to explore how effectively and uniformly the molten eutectic $NaNO_3$−KNO_3 mixture cools at varying temperatures in the quenching bath. The investigation was confined to the influence of the bath temperature, and the impact of salt mixture composition was not investigated. According to Gomez,[11] a higher melting point of $Ca(NO_3)_2$ provides better thermal stability in many high-temperature processes, making it suitable for specific industrial applications that involve elevated temperatures. Moreover, $Ca(NO_3)_2$ has a higher oxidizing potential than $NaNO_3$.[11] Chen and Zhao[12] studied the thermophysical properties of $Ca(NO_3)_2$−$NaNO_3$−KNO_3 mixtures based on weight ratios. They concluded that a 32:24:44 wt % of the above combination had the best latent heat storage capacity of 67 J/g, thereby confirming their ability to have potential thermal energy storage applications. Wu et al.[13] conducted experiments on the $NaNO_3$−KNO_3 molten salt to achieve a lower melting point and better short-term thermal stability. Fourteen different kinds of mixed molten salts were prepared by adjusting the component ratio and adding carbonates or nitrates. All of the compositions showed good short-term thermal stability in the 4-day repeated heating−cooling experiments. Babu and Prasanna Kumar[14] determined the phase distribution in quenched steel using the temperature equilibrium phase limitation method to successfully predict interfacial heat flux at the metal−quenchant interface during quenching of the AISI 4140 steel probe in water and air. A hybrid quenchant comprising 10 wt % NaCl added to 20% vol % polyalkylene glycol (PAG) solution was prepared to determine its effectiveness on distortion and crack propensity of the steel parts (Ramesh and Prabhu[15]). It was found that the hybrid solution was effective in reducing the distortion and crack propensity of steel. However, as the concentration of PAG is increased, the stability and the cooling performances of the quench media decrease, as it largely affects the encapsulation stage. Similarly, the influence of nonedible vegetable oils such as pinnata on the heat treatment of steel was examined by Ramesh and Prabhu.[16] The results showed that these oils are potential quench media for heat treatment of steel, however, only to a considerable extent. Apart from these, the addition of nanoparticles significantly affects the cooling rates of quenching heat transfer. Nanoparticles such as copper, aluminum, and multiwalled carbon nanotubes (MWCNTs) resulted in increased cooling rates at critical temperatures, as per Nayak and Prabhu.[17] Similar experiments from Nayak and Prabhu[18] conveyed that an increased concentration of copper oxide and graphene nanofluids decreased the cooling rates at critical temperatures.

Previous studies discussed different quenching agents but failed to cover the heat transfer capabilities of the $Ca(NO_3)_2$−KNO_3 quenching medium. Considering this, the cooling effectiveness and homogeneity of molten $Ca(NO_3)_2$−KNO_3 quench media of varied compositions maintained at different quench bath temperatures are evaluated in this study. This study will provide new insights and data on the heat transfer of $Ca(NO_3)_2$−KNO_3 solutions that could be used by metallurgists and material scientists to optimize the quenching process for various industrial applications.

2. EXPERIMENTAL SECTION

The effectiveness of the quenching medium's cooling was assessed by adopting an Inconel probe crafted to the dimensions of 12.5 mm in diameter and 60 mm in height, respectively, with inbuilt thermocouples attached, as seen in Figure 1. The probe was perforated with five 1 mm diameter holes through electrolytic discharge machining (EDM). A single hole was created at the midpoint of the probe up to a depth of 35 mm, followed by the remaining four holes drilled radially to 5 mm, up to depths of 10, 25, 40, and 55 mm, respectively. All of these depths are threaded to 5 mm exclusively from the top of the probe.

Precalibrated thermocouples of K-type were obtained from Phoenix Temperature & ElectroMech Manufacturing Co. WLL. Thermocouples, each of them having a measure of 1 m length, were placed into the EDM drilled holes using an 800 mm steel

https://doi.org/10.1021/acsomega.3c10262
ACS Omega 2024, 9, 17266−17275

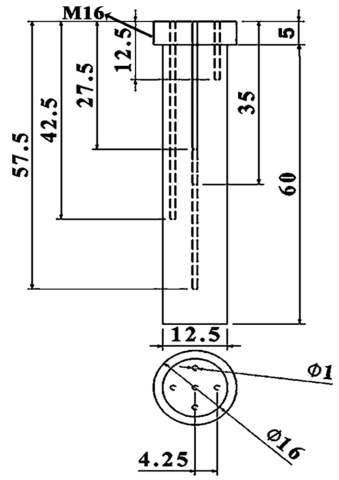

Figure 1. Inconel probe was used for experimentation.

tube, reaching into the Inconel probe. The connection between the thermocouples and the tip of the hot junction was confirmed by manually applying pressure to fasten the thermocouple onto the surface of the measuring hole. It is assured that the press fit tolerance is upheld for the thermocouple and the EDM drilled holes so that the necessary connection between the metal surface and the junction of the thermocouple is not lost during experimentation. Figure 2 gives the complete representation of

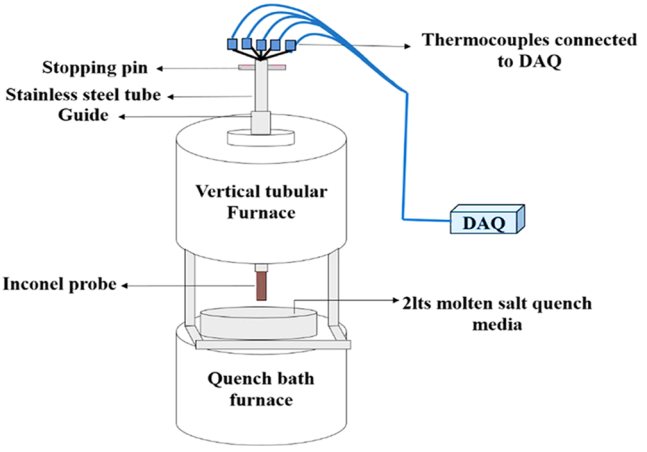

Figure 2. Quenching experiments.

the experimental setup implemented for the quenching experiment. The Inconel probe, along with the thermocouples, are fastened to the stainless-steel tube. This tube is then moved to a vertical tubular furnace. A NI-9213 data logger was connected to the thermocouples using compensation cables. This data logger was connected to a computer, which recorded the time−temperature data. This data was recorded at the rate of 10 readings per second.

The molten $Ca(NO_3)_2$−KNO_3 mixture of distinct compositions formed the 2 L quench bath. Various combinations of $Ca(NO_3)_2$−KNO_3 having a variety of compositions with corresponding bath temperatures, as listed in Table 1, were used for quenching experiments. The quench bath furnace was maintained at a specific bath temperature to melt the quench media. Next, the melting furnace was positioned directly beneath the vertical tubular furnace utilized for heating the Inconel probe, which reached a temperature of 860 °C. Subsequently, the stainless-steel probe setup was immersed in the quench bath containing the molten mixture of $Ca(NO_3)_2$−KNO_3. The guide was arranged to vertically lower the steel tube during the quenching process.

Identical quenching experiments have been conducted using steel probes made up of AISI 4140 having dimensions of 12.5 mm diameter and 60 mm length with a 5 mm M16 thread at the top. For about 20 min, the probe was maintained at an austenite temperature of 860 °C before quenching it with the molten mixture which is maintained at 300 and 350 °C. Thermocouples were placed within the probe to monitor the temperatures at specific points: one at the probe's geometric center and another 2 mm away from a depth of 30 mm. The probe was sustained in the molten bath until its geometric center reached a temperature of 20 °C above that of the quench bath. Following this, the probe was cooled via exposure to air. At a depth of 30 mm, the probe was divided into sections. One of these sections underwent metallographic polishing, followed by hardness measurement using a micro-Vickers hardness testing machine (HMV-G 20ST). A load of 0.5 kg and 15 s dwell time were employed during the hardness measurement process.

3. HEAT FLUX EVALUATION

The interfacial heat flux for the metal quenchant was determined by using temperature data from the Inconel probes. Locations in close proximity to the probe's surface compiled the cooling curve information, which was utilized in determining spatially dependent transient heat flux through the inverse heat conduction method during the quenching process. However, the location where the cooling curve data was collected was not used for inverse calculations. These thermocouple measurements served as a validation for the estimated heat flux.

$$\frac{1}{r}\frac{\partial}{\partial r}\left(kr\frac{\partial T}{\partial r}\right)+\frac{\partial}{\partial z}\left(k\frac{\partial T}{\partial z}\right)=\rho C_p\frac{\partial T}{\partial t} \quad (1)$$

The Fourier axisymmetric heat conduction equation governs quenching heat transfer in the Inconel probe given by eq 1, where k is the thermal conductivity and depends on the temperature T and ρ and C_p are the density and specific heat of the material, respectively. Figure 3 provides the cylindrical coordinates for the probe of the heat transfer model. As per

Table 1. Composition of a Molten $Ca(NO_3)_2$−KNO_3 Mixture for Quenching Experiments

composition	representation	liquidus temperature (°C)	bath temperature (°C)					
			250	300	350	400	450	500
KNO_3 (100%)	0 N	330			√	√	√	√
75% KNO_3 + 25% $Ca(NO_3)_2$	25 N	255		√	√	√	√	√
50% KNO_3 + 50% $Ca(NO_3)_2$	50 N	214	√	√	√	√	√	
25% KNO_3 + 75% $Ca(NO_3)_2$	75 N	258	√	√	√	√	√	√
$Ca(NO_3)_2$ (100%)	100 N	293		√	√	√	√	√

https://doi.org/10.1021/acsomega.3c10262
ACS Omega 2024, 9, 17266−17275

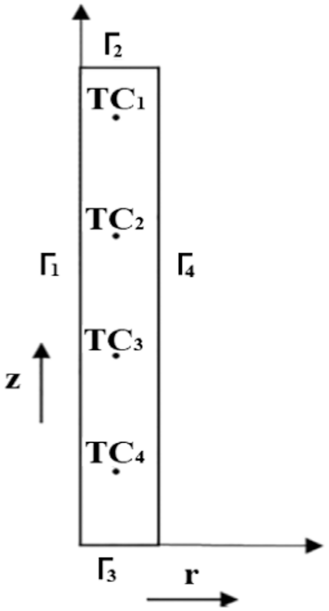

Figure 3. Inconel probe model to determine the metal−quenchant interfacial heat flux.

Table 2, r_1, r_2, r_3, and r_4 are considered as the boundary conditions at the surfaces. Prior to quenching, the probe was

Table 2. Boundary Conditions for Probe Heat Transfer

boundary surface	boundary conditions
r_1	$q = 0$ (axisymmetric)
r_2	$q = 0$
r_3	$q = 0$
r_4	$q = p_1z^3 + p_2z^2 + p_3z + p_4$

heat treated to 860 °C; therefore, at time $t = 0$, $r(r, z) = 860$ °C. This was considered the foremost requirement for resolving the inverse heat conduction model. With the implementation of these boundary conditions, the finite element method was used to solve the Fourier heat conduction equation. The axisymmetric probe model of the rectangular cross-section was discretized into almost 6000 rectangular elements having a mesh size of 0.25×0.25 mm^2. The heat transfer at the interface between the metal and the quenchant was calculated by using the thermal properties of Inconel, and these properties have been used to determine the effectiveness of cooling achieved by aqueous polymer and brine solutions used for quenching.[11] As per Table 2, the bottom and top surfaces of the probe are insulated, and r_4 is the only boundary surface through which quenching heat transfer is expected to occur. The interface heat flux r_4 is defined as a cubic function of distance z. The parameters p_1, p_2, p_3, and p_4 for the time step (ts) form the main calculation for the inverse problem. As per Ozisik and Orlande,[19] the conjugate gradient method was implemented to determine the parameters. The parameters were represented as P_{ts}.[12]

$$P_{ts} = [p_{1,ts}p_{2,ts}p_{3,ts}p_{4,ts}] \tag{2}$$

$$q(P_{ts}, z) = p_{1,ts}z^3 + p_{2,ts}z^2 + p_{3,ts}z + p_{4,ts} \tag{3}$$

z varies between 0 and 70 mm.

The thermocouple positions (r, z) TC_1, TC_2, TC_3, and TC_4 are (4.25, 7.5), (4.25, 22.5), (4.25, 37.5), and (4.25, 52.5), respectively. The temperatures measured at TC_1, TC_2, TC_3, and TC_4 are denoted as Y_1, Y_2, Y, and Y_4 respectively. The parameter values $p_{1,ts}$, $p_{2,ts}$, $p_{3,ts}$, and $p_{4,ts}$ are determined to solve the inverse problem for which objective S_{ts} was minimized (eq 4).

$$S_{ts} = \sum_{i=1}^{n}\sum_{j=1}^{m}(Y_{i,ts+j-1} - T(P_{ts})_{i,ts+j-1})^2 \tag{4}$$

Here, $Y_{i,\,ts+j-1}$ is the thermocouple location where the temperature is measured and $ts + j - 1$ is the time step. The term $T(P_{ts})$ was determined considering four upcoming time intervals during which the heat flux remained consistent. The conjugate gradient method-based inverse algorithm developed by Pranesh Rao and Prabhu[10] was used to determine the spatially dependent transient heat flux at the metal−quenchant interface. The current work used the same method.

4. RESULTS AND DISCUSSION

The quenched Inconel probe maintained at different temperatures within the quench media determined the cooling curves that were later utilized for computing the heat flux at the interface between the metal and the quenchant. The cubic equation parameters at every time step were measured using the temperatures that were determined at four different thermocouple locations, i.e., TC_1, TC_2, TC_3, and TC_4, respectively. All of these factors were employed to represent the metal−quenchant interfacial heat flux (see eq 3). Figure 4a,b shows the variation of temperature and transient parameters for $Ca(NO_3)_2$ medium, maintained at a temperature of 400 °C. During the quenching trials, similar graphs for the quench media, as reported in Table 1, were produced. Figure 4c depicts a transient fluctuation in % inaccuracy at all thermocouple sites in the probe quenched in 100 N quench medium at a bath temperature of 400 °C. The temperature at the TC_c was utilized to verify the estimated metal−quenchant interfacial heat flow. The most significant variation between the recorded and the projected temperature at TC_1, TC_2, TC_3, and TC_4 locations was 5.5% (24 °C), while quenching in 50 N salt mixture sustained at 250 °C. The highest inaccuracy at the probe's geometric center was 3.2% (24 °C). The temperature discrepancy between the actual and computed values was found to be 5.5%.

4.1. Average Heat Flux. Figure 5 displays the correlation between q_{avg} and T_{avg} observed in the Inconel probe when it underwent quenching within molten Ca $(NO_3)_2$-KNO_3 solutions preserved at varying bath temperatures. The commencement of boiling in the molten salt used for quenching signified the initial stage of heat absorption at the interface between the metal and the quenching medium. As shown in Figure 5a, q_{avg} rapidly surged to a peak value of q_{max} equivalent to a T_{avg} of T_{max} during the early quenching stage. Following that, the intensity of the heat flux diminished. The convective cooling step is the second part of the heat extraction mechanism. During this phase, the rate of heat removal was notably stagnant. The values of q_{avg} and T_{avg} transiting from the boiling to the convective stage are denoted by q_{conv} and T_{conv}, respectively.[9] The changes in the mean heat flux at critical points are primarily caused by the multiple thermal stability regimes that emerge when molten salt mixtures approach these critical points. These changes in thermal stability induce variations in heat flow and surface temperature because they give rise to chemical processes that release or absorb heat.[9,10]

https://doi.org/10.1021/acsomega.3c10262
ACS Omega 2024, 9, 17266−17275

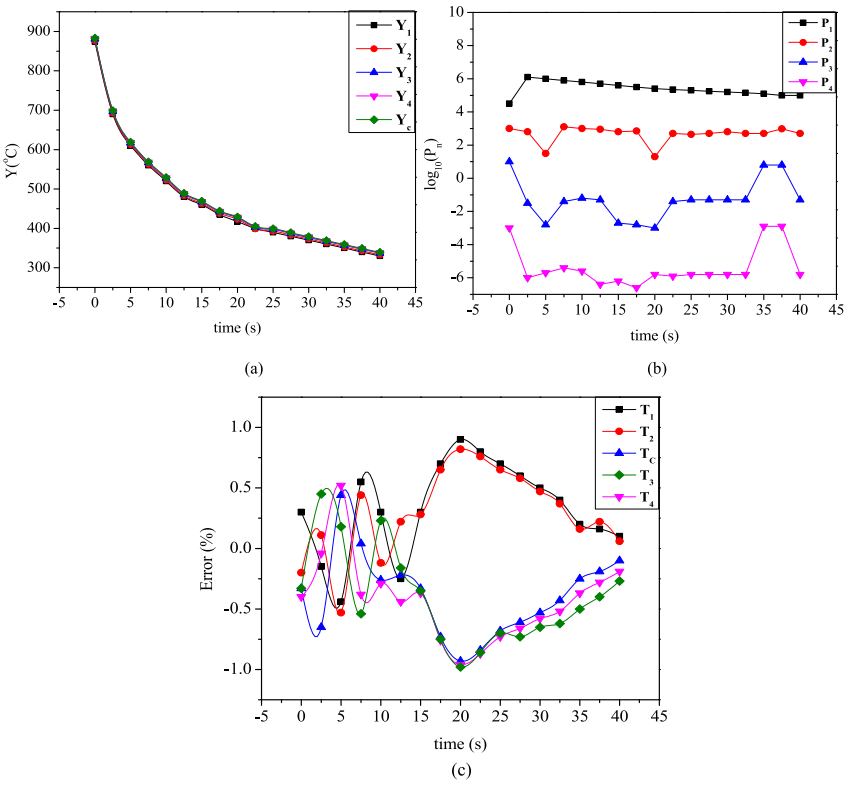

Figure 4. Variation of (a) temperature, (b) transient heat flux, and (c) transient variation of % error at thermocouple positions for the molten Ca $(NO_3)_2$ quenching medium at 400 °C.

4.2. Evaluation of Critical Points in Thermocouple for Varying Composition and Bath Temperature. The maximum rate of heat removal throughout the nucleate boiling phase and the shift from nucleate to convective cooling were selected as the crucial stages to evaluate the quench media's ability to cool down.[9] The terminologies q_{max}, T_{max}, q_{conv}, and T_{conv} have been utilized to describe the quench performance of molten $Ca(NO_3)_2$–KNO_3 mixtures. Results from quenching experiments were used to construct Figure 6a–d. The data for all contour plots in Figure 6 are included in Table 3. The highest average heat transfer decreased with the increase in the KNO_3 content and temperature of the quenching medium. T_{max} rose as the KNO_3 content and bath temperature in the quenching medium increased. For bath temperatures of >400 °C, q_{conv} remained practically identical across all compositions. q_{conv} improved with the KNO_3 content in the molten salt medium at bath temperatures under 350 °C. With the increase in both the concentration of KNO_3 and the temperature of the quenching medium, there was a corresponding rise in T_{conv}. By altering the composition of the molten $Ca(NO_3)_2$–KNO_3 mixtures, it is possible to attain maximum cooling efficiency.

Upon quenching, greater q_{max} and q_{conv} values and lower T_{conv} values contribute to enhanced hardness in the quenched steel portion. A greater q_{max} value suggests a faster cooling rate, preventing the pearlitic tip of steel on the TTT diagram. In the TTT diagram, T_{max} is expected to be near but lower than the pearlite tip of the steel. Reduced T_{conv} and higher q_{conv} values prevent bainitic transition following quenching of the steel components. Greater peak heat flux provides faster heat transfer rates until the convective cooling period begins. Increasing heat transfer rates across T_{max} and T_{conv} temperatures inhibits austenite transition to bainite and pearlite.

4.3. Steel Probe Quenching. The reduction in hardness in the AISI 4140 steel probe quenched in 75 and 50 N quench media sustained at 310 °C was ascribed to a considerable drop in the magnitude of q_{max}, as seen in Figure 7. T_{max} increased, whereas q_{conv} and T_{conv} did not alter significantly. The rise in the value of q_{conv} was connected to the growth in the probe's hardness quenched in 50 and 25 N quench medium. This stimulated the cooling rate all through the convective cooling stage, suppressing the bainitic transition of austenite. In this situation, increasing the value of q_{max} had no meaningful influence on the hardness of the steel portion.

The variation of q_{max} significantly influenced the steel probe's hardness quenched in a $Ca(NO_3)_2$–KNO_3 mixture, which was maintained at 350 °C. The early occurrence of the convective cooling phase restricted the benefits that could have been achieved due to high q_{conv} at higher concentrations of KNO_3 in the molten bath. This is unlikely to take place in the molten bath maintained at 310 °C and is indicated by the higher values of T_{conv}.

4.4. Uniformity of the Steel Probe Quenching Cooling. Equation 5 has been used to estimate the normalized energy at the interface between the metal and the quenchant. The energy extracted during quenching per unit area was determined by integrating the nodal quench heat flux over the first 50 s.

$$E_z = \frac{\int_0^{50} q(t, z)\mathrm{d}t}{\max\left[\int_0^{50} q(t, z)\mathrm{d}t\right]} \quad (5)$$

The unevenness in the heat removal across the surface of the probe is generally reflected in the spatial variation of the normalized heat energy (Figure 8). The quenched steel parts typically tend to experience nonuniform hardness and

https://doi.org/10.1021/acsomega.3c10262
ACS Omega 2024, 9, 17266−17275

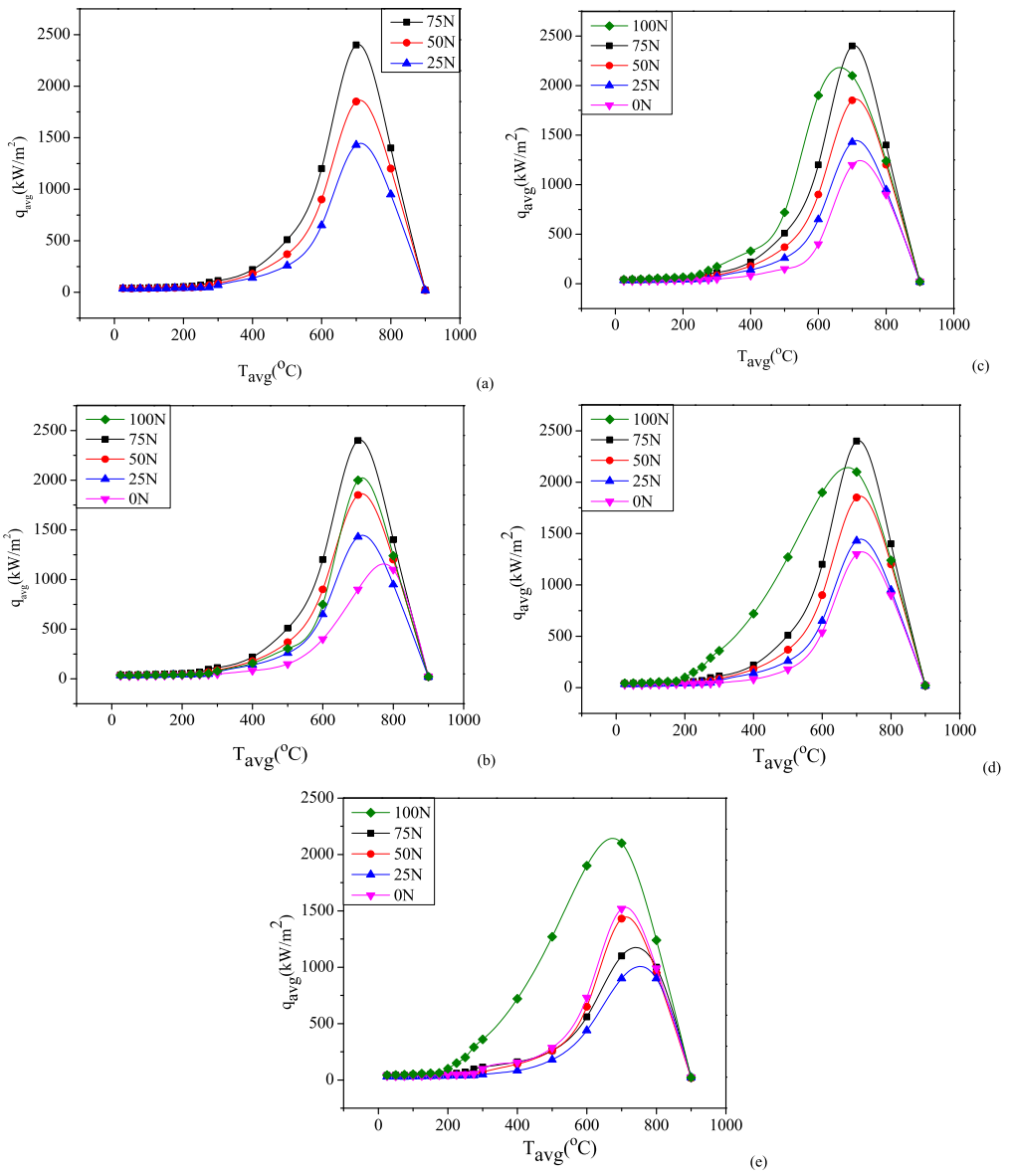

Figure 5. Variation of q_{avg} w.r.t. T_{avg} for the Inconel quench probe in a molten Ca $(NO_3)_2$-KNO_3 mixture at (a) 300 °C, (b) 350 °C, (c) 400 °C, (d) 450 °C, and (e) 500 °C.

deficiencies because of this spatial variation. An increase in the KNO_3 concentration in the molten bath resulted in a decreased cooling uniformity along the surface of the Inconel probe.

4.5. Thermochemical Decomposition of the Molten Bath. The Inconel probe underwent quenching heat transfer in two phases: the boiling phase and the convective cooling phase. During the boiling phase, the decomposition of the molten $Ca(NO_3)_2$–KNO_3 mixture leads to heat extraction at the hot probe quenching surface. The heat extraction rate largely depends on the endothermic reversible chemical reaction in the boiling phase, given by eqs 6 and 7 and eqs 8 and 9, respectively. The other major contributors to the boiling phase quench heat transfer were free convection and turbulence due to the evolution of the gas. Nonetheless, the decomposition of nitrates is the primary reason for the conventional heat extraction mechanism at the probe surface.

$$Ca(NO_3)_2 = Ca + 2NO_2 + O_2 \quad (6)$$

$$2Ca(NO_3)_2 = 2Ca + 4NO_2 + 2O_2 \quad (7)$$

This discussion on thermodynamic decomposition draws on the data and work presented by Stern,[20] which analyzed the decomposition rates and reactions of various salts. The Ca $(NO_3)_2$ decomposes to liquid by melting and maintains its stability at 550 °C and then begins to decompose at 650 °C. A pseudoequilibrium is developed between liquid and air for the temperature ranging between 600–700 °C with the solution containing Ca and NO_2 being temperature dependent.

$$KNO_3 = KNO_2 + \frac{1}{2}O_2 \quad (8)$$

$$2KNO_3 = K_2O + 2NO_2 + \frac{1}{2}O_2 \quad (9)$$

KNO_3 does not undergo decomposition during melting and is stable in air up to a temperature of at least 525 °C. When KNO_3 is heated in air at 650 °C, it decomposes and sets up a quasi-equilibrium between the temperatures 600–750 °C. It could be observed from eqs 7–9 that nitrate oxide reactions tend to occur

https://doi.org/10.1021/acsomega.3c10262
ACS Omega 2024, 9, 17266−17275

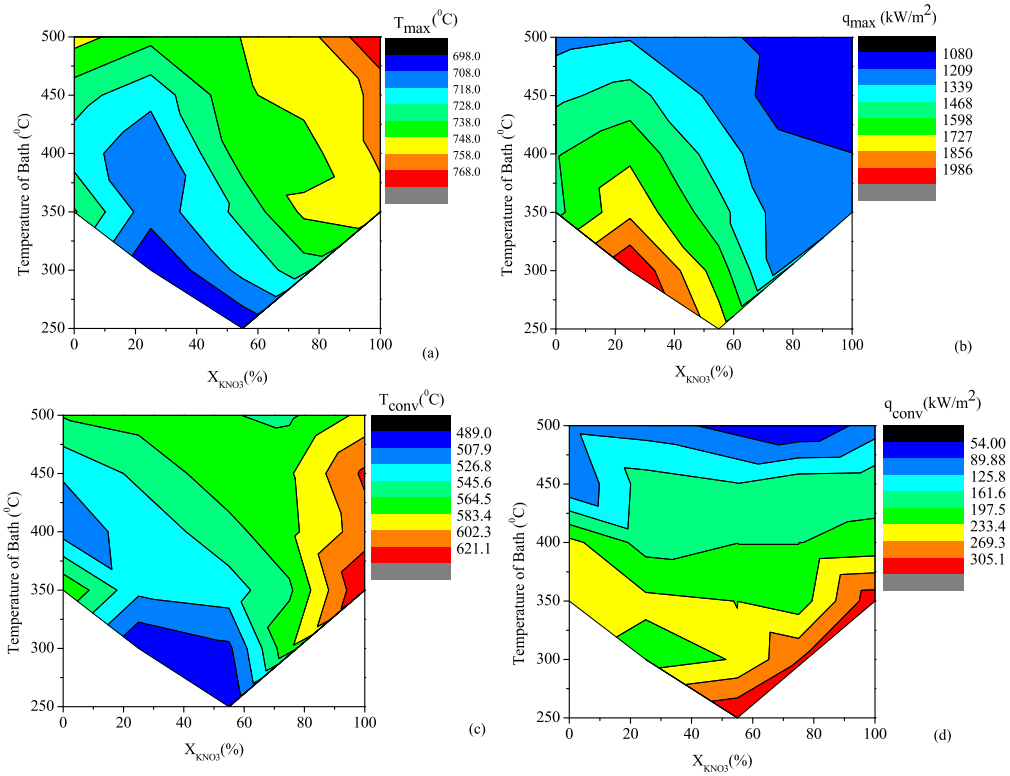

Figure 6. Contour plots for (a) T_{max}, (b) q_{max}, (c) T_{conv}, and (d) q_{conv} for different compositions and bath temperatures in the $Ca(NO_3)_2$−KNO_3 mixture.

Table 3. Heat Flux Parameters for Different Compositions and Bath Temperatures in the $Ca(NO_3)_2$−KNO_3 Mixture

concentration, KNO_3 (%)	T_b (°C)	T_{max} (°C)	q_{max} (kW/m^2)	T_{conv} (°C)	q_{conv} (kW/m^2)
50	250	696	1739	481	341
50	300	712	1649	504	236
50	350	719	1500	537	233
50	400	739	1354	550	197
50	450	747	1296	573	163
75	300	733	1296	580	301
75	350	737	1223	561	213
75	400	744	1224	572	197
75	450	751	1155	581	184
75	500	753	1114	556	54
25	300	686	2070	489	215
25	350	712	1826	528	242
25	400	710	1663	532	183
25	450	721	1521	550	179
25	500	736	1328	568	108
0	350	739	1565	573	263
0	400	702	1588	519	245
0	450	732	1418	517	91
0	500	741	1266	566	117
100	350	754	1214	631	329
100	400	755	1183	612	205
100	450	760	1136	611	187
100	500	766	1033	578	108

only beyond 750 °C. Therefore, the influence of such reactions on the extraction of heat during quenching can be considered negligible.

The variation in energy and enthalpy during the nitrite−nitrate reactions can be observed in Figure 9. Figure 9a shows

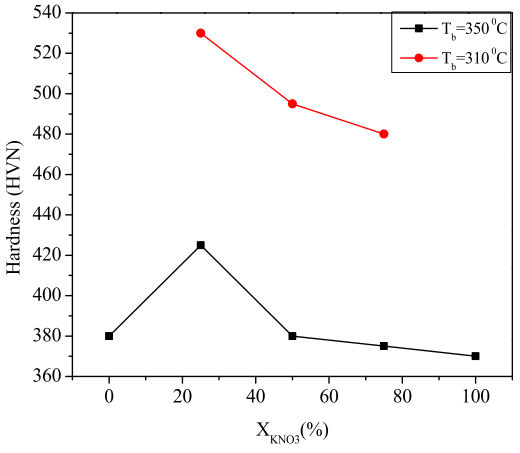

Figure 7. Hardness of the AISI 4140 steel probe in molten $Ca(NO_3)_2$−KNO_3 mixture for varying composition of KNO_3 at temperatures of 310 and 350 °C, respectively.

that the standard changes occurring in the decomposition of KNO_3 were higher than that for $Ca(NO_3)_2$. Also, the decomposition of $Ca(NO_3)_2$ is more spontaneous than that of KNO_3 for a given temperature. Due to this, the quenched $Ca(NO_3)_2$ eutectic mixture observes an extended boiling phase. As shown in Figure 9b, the equilibrium constant (K_{eq}) for the decomposition of $Ca(NO_3)_2$ was higher than that of KNO_3. All of this indicated that for a given temperature, the rate of decomposition, pressure, and surface temperature for $Ca(NO_3)_2$ was altogether higher than the KNO_3 decomposition rate.

$$K_{eq} = \frac{[MNO_2][O_2]^{1/2}}{[MNO_3]} \quad (10)$$

https://doi.org/10.1021/acsomega.3c10262
ACS Omega 2024, 9, 17266−17275

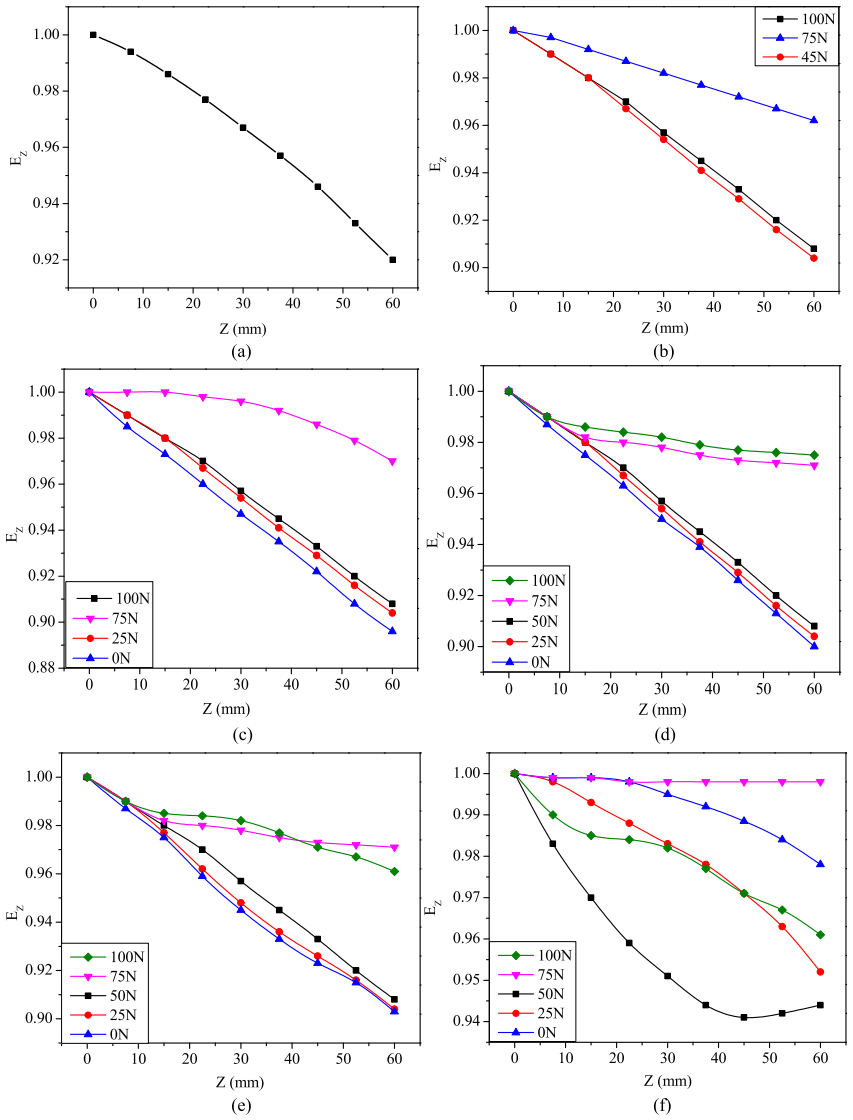

Figure 8. Plots for normalized heat energy for the $Ca(NO_3)_2$–KNO_3 mixture at temperatures of (a) 250 °C, (b) 300 °C, (c) 350 °C, (d) 400 °C, (e) 450 °C, and (f) 500 °C.

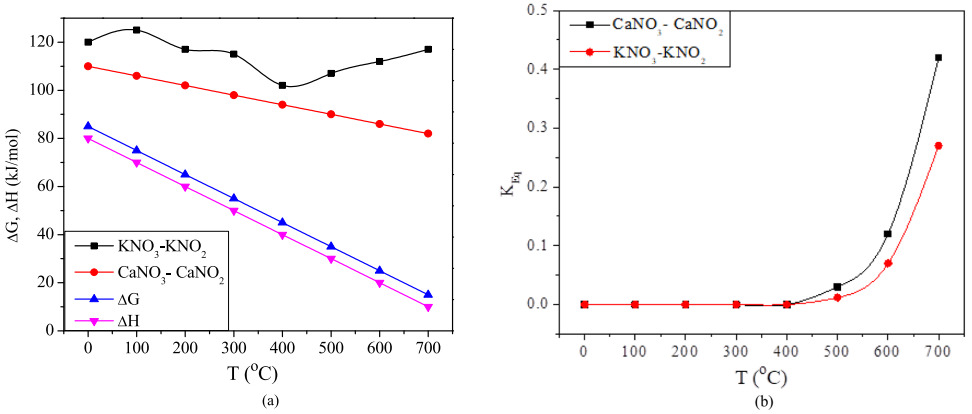

Figure 9. (a) Variation in enthalpy and Gibbs free energy with respect to surface temperature. (b) Variation of the equilibrium constant for the decomposition of Ca $(NO_3)_2$ and KNO_3.

As the bath temperature increases, the nitrite–nitrate ratio also increases, and as per eq 10, the nitrite salt resisted decomposition in the presence of nitrite in the molten bath. It is important to mention that, at the boiling phase, nitrite concentration increases close to the quench probe surface. This eventually leads to the formation of a concentration barrier that diminishes the decomposition rate of nitrites. Apparently, the end of the boiling phase occurs when the heat energy developed

https://doi.org/10.1021/acsomega.3c10262
ACS Omega 2024, 9, 17266−17275

at the probe surface falls below the level required for nitrite decomposition.

5. CONCLUSIONS

The influence of the bath temperature and composition on the cooling performance of Ca $(NO_3)_2$-KNO_3 has been investigated using AISI 4140 and Inconel quench probes. The experiments draw the following conclusions:

- The contour plots for varying q_{max}, T_{max}, q_{conv}, and T_{conv} were developed to analyze the cooling performance of $Ca(NO_3)_2$−KNO_3 quench media for different bath temperatures.
- As the concentration of KNO_3 decreased in the quench media, the cooling performance of the Inconel probe, determined by the degree of uniformity, increased.
- An increase in the nitrite concentration near the quench probe surface during the boiling phase reduced the rate of nitrate decomposition. This decomposition occurs mainly because of the endothermic reaction that happens during quench boiling.
- The convection cooling phase initiates as the supply of heat by the probe tends to become insufficient for nitrate decomposition. This is primarily attributed to the high concentration of nitrites forming a barrier at the surface of the quench probe.
- The investigation of heat transfer in $Ca(NO_3)_2$-KNO_3 molten salt combinations may have a few drawbacks. Among these is the corrosive nature of the molten salt, which frequently causes damage to the experimental setup. Corrosion causes contamination of the salt mixture, reducing the precision of heat transfer measurements. Furthermore, molten salt mixtures display complicated phenomena such as temperature phase transitions and heat transfer properties. These complications frequently pose problems in the experimental design and data interpretation.

AUTHOR INFORMATION

Corresponding Author

Abdul Aabid − *Department of Engineering Management, College of Engineering, Prince Sultan University, Riyadh 11586, Saudi Arabia;* orcid.org/0000-0002-4355-9803; Email: aaabid@psu.edu.sa

Authors

Jaimon D. Quadros − *Department of Mechanical Engineering, University of Bolton, RAK Academic Center, 16038 Ras Al Khaimah, UAE*

Sher Afghan Khan − *Department of Mechanical and Aerospace Engineering, International Islamic University Malaysia, Kuala Lumpur 53100 Selangor, Malaysia*

Ma Mohin − *School of Engineering, University of Bolton, Bolton BL3 5AB, U.K.*

Yakub I. Mogul − *National Centre for Motorsport Engineering, University of Bolton, Bolton BL3 5AB, U.K.*

Muneer Baig − *Department of Engineering Management, College of Engineering, Prince Sultan University, Riyadh 11586, Saudi Arabia*

Omar Shabbir Ahmed − *Department of Engineering Management, College of Engineering, Prince Sultan University, Riyadh 11586, Saudi Arabia*

Complete contact information is available at: https://pubs.acs.org/10.1021/acsomega.3c10262

Notes

The authors declare no competing financial interest.

ACKNOWLEDGMENTS

This research was supported by the Structures and Materials (S&M) Research Lab of Prince Sultan University. Furthermore, the authors acknowledge the support of Prince Sultan University for paying the article processing charges (APC) of this publication.

REFERENCES

(1) *Handbook of Quenchants and Quenching Technology*; Totten, G. E.; Bates, C. E.; Clinton, N. A., Eds.; ASM International: Cleveland, 1993.

(2) Narazaki, M.; Totten, G. E.; Webster, G. M. Hardening by Reheating and Quenching. In *Handbook of Residual Stress and Deformation of Steel*, 1st ed.; ASM International: Cleveland, 2002; pp 248−295.

(3) ASM Handbook Committee. *ASM Handbook. Volume 4: Heat Treating*, 8th ed.; ASM International: Cleveland, 1969.

(4) Lantelme, F.; Groult, H.; Mosqueda, H.; Magdidnier, P. L.; Chavanne, H.; Monteux, V.; Maurin Pierre, P. Salt Bath Thermal Heat Treating and Nitriding. In *Molten Salts Chemistry from Lab to Applications*, 1st ed.; Lantelme, F.; Groult, H., Eds.; Elsevier, 2013; pp 101−130.

(5) Dexter, G. W. Hardening High Speed Steels: Metallurgical Benefits of Salts.

(6) Torkamani, H.; Raygan, S.; Rassizadehghani, J. Comparing Microstructure and Mechanical Properties of AISI, D2 Steel After Bright Hardening and Oil Quenching. *Mater. Des.* **2014**, *54*, 1049−1055.

(7) Luty, W. Cooling Media and Their Properties. In *Quenching Theory and Technology*, 2nd ed.; Lisicic, B.; Tensi, H. M.; Canale, L. C., Eds.; CRC Press, 2010; pp 359−445.

(8) Dubal, G. P. Salt Bath Quenching. *Adv. Mater. Process.* **1999**, *156*, H23−H28.

(9) Yagov, V. V.; Zabirov, A. R.; Kaban'kov, O.; Kabankov, O. N. Heat Transfer During Cooling of High Temperature Spheres in Subcooled Water at different Pressures. *Int. J. Heat Mass Transfer* **2017**, *110*, 219−230.

(10) Pranesh Rao, K. M.; Prabhu, K. N. Effect of Bath Temperature on Cooling Performance of Molten Eutectic $NaNO_3$−KNO_3 Quench Medium for Martempering of Steels. *Metall. Mater. Trans. A* **2017**, *48*, 4895−4904.

(11) Gomez, J. C.; Calvet, N. $Ca(NO_3)_2$—$NaNO_3$—KNO_3 Molten Salt Mixtures for Direct Thermal Energy Storage Systems in Parabolic Trough Plants. *J. Sol. Energy Eng.* **2013**, *135*, 021016.

(12) Chen, Y. Y.; Zhao, C. Y. Thermophysical properties of $Ca(NO_3)_2$-$NaNO_3$-KNO_3 mixtures for heat transfer and thermal storage. *Sol. Energy* **2017**, *146*, 172−179.

(13) Wu, Y.-t.; Li, Y.; Ren, N.; Ma, C. F. Improving the thermal properties of $NaNO_3$-KNO_3 for concentrating solar power by adding additives. *Sol. Energy Mater. Sol. Cells* **2017**, *160*, 263−268.

(14) Babu, K.; Prasanna Kumar, T. S. Comparison of Austenite Decomposition Models During Finite Element Simulation of Water Quenching and Air Cooling of AISI 4140 Steel. *Metall. Mater. Trans. B* **2014**, *45* (4), 1530−1544.

(15) Ramesh, G.; Prabhu, K. N. Comparative Study of Wetting and Cooling Performance of Polymer − Salt Hybrid Quench Medium with Conventional Quench Media. *Exp. Heat Transfer* **2015**, *28*, 464−492.

(16) Ramesh, G.; Prabhu, K. N. Wetting kinetics, kinematics, and heat transfer characteristics of Pongamia pinnata vegetable oil for industrial heat treatment. *Appl. Therm. Eng.* **2014**, *65* (1−2), 433−446.

(17) Nayak, U. V.; Prabhu, K. N. Heat transfer during immersion quenching in MWCNT nanofluids. *Mater. Sci. Forum* **2015**, *830*−*831*, 172−176.

(18) Nayak, U. V.; Prabhu, K. N. Heat transfer and quench performance of aqueous CuO nanofluids during immersion quenching. *Int. J. Microstruct. Mater. Prop.* **2016**, *11*, 186−202.
(19) Ozisik, M. N.; Orlande, H. R. B. Techniques for Solving Inverse Heat Transfer Problems. In *Inverse Heat Transfer: Fundamentals and Applications*; Taylor and Francis, 2000; pp 35−114.(20) K.H. Stern. High Temperature Properties and Thermal Decomposition of Inorganic Salts with Oxyanions, CRC Press, Boca Raton, 2001.
(20) Stern, K. H. High Temperature Properties and Thermal Decomposition of Inorganic Salts with Oxyanions. CRC Press: Boca Raton, 2001.

https://doi.org/10.1021/acsomega.3c10262
ACS Omega 2024, 9, 17266−17275